Transverse correlations in triphoton entanglement: Geometrical and physical optics

Jianming Wen,[1,*] P. Xu,[2] Morton H. Rubin,[1] and Yanhua Shih[1]
[1]*Physics Department, University of Maryland, Baltimore, Maryland 21250, USA*
[2]*National Laboratory of Solid State Microstructures, Nanjing University, Nanjing, 210093, People's Republic of China*
(Received 30 April 2007; published 30 August 2007)

The transverse correlation of triphoton entanglement generated within a single crystal is analyzed. Among many interesting features of the transverse correlation, they arise from the spectral function F of the triphoton state produced in the parametric processes. One consequence of transverse effects of entangled states is quantum imaging, which is theoretically studied in photon counting measurements. Klyshko's two-photon advanced-wave picture is found to be applicable to the multiphoton entanglement with some modifications. We found that in the two-photon coincidence counting measurement by using triphoton entanglement, although the Gaussian thin lens equation (GTLE) holds, the imaging shown in coincidences is obscure and has a poor quality. This is because of tracing the remaining transverse modes in the untouched beam. In the triphoton imaging experiments, two kinds of cases have been examined. For the case that only one object with one thin lens is placed in the system, we found that the GTLE holds as expected in the triphoton coincidences and the effective distance between the lens and imaging plane is the parallel combination of two distances between the lens and two detectors weighted by wavelengths, which behaves as the parallel combination of resistors in the electromagnetism theory. Only in this case, a point-point correspondence for forming an image is well-accomplished. However, when two objects or two lenses are inserted in the system, though the GTLEs are well-satisfied, in general a point-point correspondence for imaging cannot be established. Under certain conditions, two blurred images may be observed in the coincidence counts. We have also studied the ghost interference-diffraction experiments by using double slits as apertures in triphoton entanglement. It was found that when two double slits are used in two optical beams, the interference-diffraction patterns show unusual features compared with the two-photon case. This unusual behavior is a destructive interference between two amplitudes for two photons crossing two double slits.

DOI: 10.1103/PhysRevA.76.023828 PACS number(s): 42.50.Dv, 42.25.Fx, 42.82.Cr, 42.30.Kq

I. INTRODUCTION

Since the seminal work of Einstein, Podolsky, and Rosen [1], entangled states of two or more quantum particles have become the heart of many major paradoxes associated with the interpretation of quantum mechanics [2]. Over the last two decades, correlated photon pairs created in optical spontaneous parametric down-conversion (SPDC) [3] and EIT-based systems [4] have been extensively studied in both theories and experiments. Many applications for these entangled photon pairs range from the foundations of quantum mechanics [5], optical measurements [6], spectroscopy [7], imaging [8–11], and lithography [12,13], to quantum information processing [14]. Recently, there has been great interest in exploring the generation and properties of multiparticle entanglement since the pioneering work of Greenberger, Horne, and Zeilinger (GHZ) [15]. The multiparticle entanglement has also been assumed an important place in the practical development of quantum cryptography techniques and in the construction of basic elements of quantum teleportation to serve as a part of the quantum communication and quantum computing process [16]. A number of proposals for generating such states have been put forward [17,18]. To date, however, most theories and experiments have concentrated on the effects of the frequency phase matching for $N \geq 3$ particle entanglement. In this paper we present a theoretical treatment of the transverse correlations in triphoton generation proposed in Ref. [18] with emphasis on the geometrical and physical optics properties of the triphoton amplitude.

By taking advantage of the entangled nature of paired photons created from SPDC, Pittman *et al.* [9] proved the possibility of reproducing, nonlocally, the ghost image of an object and found that the location of the image plane was governed by a two-photon Gaussian thin lens equation (GTLE). This pioneering ghost imaging work was soon followed by another experimental development; Strekalov *et al.* demonstrated the ghost interference-diffraction pattern of a double slit [11]. The proof-of-principle experimental demonstration of quantum lithography was reported in [13]. The experimental results confirmed that the two-photon interference-diffraction pattern has a spatial interference modulation period smaller and a diffraction pattern width narrower, by a factor of 2, than in the classical case.

Stimulated by the two-photon quantum imaging, one may raise the question: do there always exist GTLEs which are satisfied for the multiphoton quantum imaging? If so, what kind of imaging properties will they present? For the triphoton entangled state, in this paper we found that the GTLEs are always established but high-resolution images are not always attained. Performing the two-photon imaging by making use of triphoton sources, it was found that the image governed by GTLE becomes obscure and this is different from the ghost imaging implemented by paired photon sources such as SPDC [9,10]. Under different arrangements in the triphoton imaging process, we found that if only one

*jianm1@umbc.edu

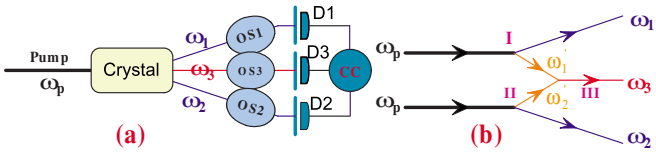

FIG. 1. (Color online) (a) Photon counting measurements. "CC" represents the coincidence counter and "OS"s are the optical systems, respectively. Dj (j=1,2,3) are point photodetectors. (b) Triphoton interaction. Processes I and II denote two parametric down-conversions while III is an up-conversion.

object with one thin lens is placed in either of the optical beams, the ghost image has a better resolution in the imaging plane. The distance from the lens to the imaging plane is the effective length which is a parallel combination of the distances between the lens and two detectors weighted by wavelengths, and this behaves as a parallel combination of resistors in the electromagnetism theory. However, if two objects are placed in the optical beams, in general, it is not always possible to obtain high-quality images in the imaging planes [for experimental setup see Fig. 1(a)]. The reason is that the *point-point* correspondence for forming an image turns now to be a *point-spot* relationship. In general, to image one object with one lens in the multiphoton entanglement, the high-resolution image can be formed in the imaging plane and the two-photon advanced-wave model proposed by Klyshko [19] provides an intuitive picture for understanding the imaging process, except that the distance between the lens and imaging plane should be interpreted as the effective length which behaves as the parallel combination of resistors in the electromagnetism theory. In principle, to image more than one object or image one object with more than one lens in the multiphoton entanglement, in the imaging planes generally blurred images can be observed in the coincidences. By carefully choosing the experimental parameters, the images may be approximately reduced to independent images of each object.

To further understand the transverse correlation of triphoton entanglement, we also studied the quantum ghost interference-diffraction experiments in which double slits are placed as apertures in the optical beams. It was found that when placing two double slits in the experiment, the ghost interference-diffraction patterns will exhibit unusual features, which are different from the patterns obtained using one double slit. This unusual behavior is caused by the destructive interference between two amplitudes for two photons to cross two double slits.

The paper is organized as follows. Because the imaging properties are determined by both the transfer functions of optical systems placed in front of the detectors and the spectral function of the triphoton state, we begin with modeling the spectral function F of the triphoton generation proposed in Ref. [18] in Sec. II. In Sec. III, the triphoton geometrical optics will be presented and the quantum imaging will be discussed for several cases. These include the single-photon detection, two-photon imaging, and triphoton imaging under different experimental setups. In Sec. IV, we will consider the quantum ghost interference-diffraction experiments by using double slits as apertures and three kinds of experimental situations will be examined. In the end, the conclusion will be given.

II. SPECTRAL FUNCTION OF TRIPHOTON STATE

The triphoton state considered here is generated by two SPDCs and the sum frequency generation (SFG) of two idler beams, see Fig. 1(b). All three interactions occur within a single crystal. This method exploits a phase matching retracing behavior in one crystal and it makes it possible to generate a triphoton state from a single pump beam [20]. For simplicity, we assume that a monochromatic pump laser with angular frequency Ω_p is incident on such a noncentrosymmetric crystal and propagates along the longitudinal axis z. In the experiment, one can use filters to achieve an approximately cw pump mode. The length of the crystal is L and effective cross section area is A. In SPDC a pump photon is annihilated and a paired signal and idler with angular frequency ω_s and ω_i are produced. Similarly in SFG a pair of idler photons are annihilated to produce an up-conversion photon with angular frequency ω_u [Fig. 1(b)]. In SPDC, the pump field is many orders of magnitude larger than the generated fields and is taken to be classical, while the signal and idler beams are quantized. In SFG all three fields are treated quantum mechanically. Considering the weak nonlinear interaction, we assume that the perturbation theory is suitable to study the optical properties of the system.

In the interaction picture, the effective Hamiltonian for the optical parametric processes in a nonlinear crystal is given by

$$\mathcal{H} = \int_V d^3r \frac{\varepsilon_0 \chi^{(2)}}{2} E_a E_b E_c, \tag{1}$$

where V is the interaction volume of the crystal illuminated by the pump laser E_p and $\chi^{(2)}$ is the second-order nonlinear susceptibility. The positive frequency part of the quantized field inside the crystal is

$$E_j^{(+)} = \sum_{\vec{k}_j} E_j e^{i(\vec{k}_j \cdot \vec{r} - \omega_j t)} a_{\vec{k}_j}, \tag{2}$$

where the dispersion relation is $|\vec{k}_j| = \omega_j n_j / c$, n_j is the refractive index, $E_j = i\sqrt{\hbar \omega_j / 2\varepsilon_0 n_j^2 V_Q}$, and V_Q is the quantization volume.

In keeping only the terms of interest, the calculation of the triphoton state to third order in the perturbation theory gives

$$|\Psi\rangle = \left(\frac{-i}{\hbar}\right)^3 \int_{-\infty}^{\infty} dt_{\mathrm{I}} \int_{-\infty}^{\infty} dt_{\mathrm{II}} \int_{-\infty}^{\infty} dt_{\mathrm{III}} \mathcal{T}[\mathcal{H}(t_{\mathrm{I}})\mathcal{H}(t_{\mathrm{II}})\mathcal{H}(t_{\mathrm{III}})]|0\rangle$$

$$= \beta \sum_{\vec{k}_{s1}} \sum_{\vec{k}_{s2}} \sum_{\vec{k}_u} F(\vec{k}_{s1}, \vec{k}_{s2}, \vec{k}_u) a^\dagger(\vec{k}_{s1}) a^\dagger(\vec{k}_{s2}) a^\dagger(\vec{k}_u)|0\rangle, \tag{3}$$

where $\mathcal{T}$ is the time-ordering operator for three parametric processes, $\beta = [-\pi i \varepsilon_0 \chi^{(2)} V_Q]^3 (E_p E_s E_i^2)^2 E_u$ is the parametric gain index, and F is called the *spectral function*, which is defined by

$$F(\vec{k}_{s1},\vec{k}_{s2},\vec{k}_u)=\sum_{\vec{k}_{i1}}\sum_{\vec{k}_{i2}}\Phi(\delta k_{\mathrm{I}}L)\Phi(\delta k_{\mathrm{II}}L)\Phi(\delta k_{\mathrm{III}}L)$$
$$\times H(\vec{\alpha}_{s1}+\vec{\alpha}_{i1})H(\vec{\alpha}_{s2}+\vec{\alpha}_{i2})H(\vec{\alpha}_u-\vec{\alpha}_{i1}-\vec{\alpha}_{i2})$$
$$\times\delta(\Omega_p-\omega_{s1}-\omega_{i1})\delta(\Omega_p-\omega_{s2}-\omega_{i2})$$
$$\times\delta(\omega_{i1}+\omega_{i2}-\omega_u). \quad (4)$$

In Eq. (4), Φ is called the longitudinal detuning function which is the z integral from $-L$ to 0 over the length of the crystal, i.e.,

$$\Phi(x)=\frac{1-e^{-ix}}{ix}. \quad (5)$$

The phase mismatching in the longitudinal z direction for three parametric processes is $\delta k_{\mathrm{I}}=k_p-k_{s1}-k_{i1}$, $\delta k_{\mathrm{II}}=k_p-k_{s2}-k_{i2}$, and $\delta k_{\mathrm{III}}=k_{i1}+k_{i2}-k_u$. These longitudinal detuning functions determine the natural spectral widths of the two-photon states in SPDC and the triphoton, respectively. The integrals over the area A of the intersection of the beam cross section and the crystal give the transverse detuning functions, which take the form of

$$H(\vec{\alpha})=\frac{1}{A}\int_A d^2\rho e^{-\vec{\alpha}\cdot\vec{\rho}}, \quad (6)$$

where we have assumed that A is independent of z. The time integrals give the Dirac δ functions in the steady-state approximation. The transverse detuning function H depends on the transverse components of the wave vectors. In the limit that the area of the pump beam is large enough so that the diffraction may be neglected, $H(\vec{\alpha})=\delta(\vec{\alpha})$ can be reached. Under such an approximation, the generated modes are correlated in pairs. In most experiments, the range of the transverse modes is limited by placing pin holes in the beam pathways. In the limit of infinite crystal length and large cross area, we have perfect phase matching conditions in energy and momentum for three parametric generations.

Before proceeding, we consider the phase mismatching in the longitudinal axis. We approximate the frequencies as small deviations around the corresponding central frequencies, i.e., $\omega_{s1}=\Omega_{s1}+\nu_1$ and $\omega_{s2}=\Omega_{s2}+\nu_2$ where the range of frequencies reaching each detector, ν_j, is limited so that $|\nu_j|\ll\Omega_{sj}$. This approximation is valid only to perfect phase matching. Expanding the wave vectors to first order, we obtain

$$k_{sj}=K_{sj}+\frac{\nu_j}{u_{sj}}-\frac{\alpha_{sj}^2}{2K_{sj}}, \quad (7)$$

where K_{sj} is the central wave number, u_{sj} is the group velocity of the sj beam, and $\vec{\alpha}$ is the transverse component of the wave vector, respectively. To maximize the output intensities of the interaction, the crystal is cut so that for $j=1,2$

$$K_{s1}+K_{i1}=k_p,\quad K_{s2}+K_{i2}=k_p,\quad K_{i1}+K_{i2}=K_u,$$
$$\Omega_{s1}+\Omega_{i1}=\Omega_p,\quad \Omega_{s2}+\Omega_{i2}=\Omega_p,\quad \Omega_{i1}+\Omega_{i2}=\Omega_u. \quad (8)$$

Throughout this paper we shall denote the central frequencies and wave numbers by capital letters as in Eqs. (7) and (8). Thus the phase mismatchings δk_j now become

$$\delta k_{\mathrm{I}}=-\nu_1 D_{11}+\frac{\alpha_{s1}^2}{2K_{s1}}+\frac{\alpha_{i1}^2}{2K_{i1}},$$
$$\delta k_{\mathrm{II}}=-\nu_2 D_{22}+\frac{\alpha_{s2}^2}{2K_{s2}}+\frac{\alpha_{i2}^2}{2K_{i2}},$$
$$\delta k_{\mathrm{III}}=-\nu_1 D_{13}-\nu_2 D_{23}-\frac{\alpha_{i1}^2}{2K_{i1}}-\frac{\alpha_{i2}^2}{2K_{i2}}+\frac{\alpha_u^2}{2K_u}, \quad (9)$$

where $D_{jj}=1/u_{sj}-1/u_{ij}$ and $D_{j3}=1/u_{ij}-1/u_u$ $(j=1,2)$ and $D_{jk}L$ is the difference in time for the j and k beams to cross the crystal.

III. TRIPHOTON GEOMETRICAL OPTICS

The interesting properties of a triphoton state, especially the transverse correlation, lead to many potential applications such as quantum imaging and lithography. In this section, we will focus on the transverse effects in a triphoton state by implementing the photon coincidence counting measurement. We will show how the singles, two~photon coincidence, and triphoton coincidence counting rates are determined by the spectral function F and the optical systems placed between the crystal and the detectors. We will concentrate on the experiments schematically shown in Fig. 1(a), where a strong cw pump beam incident on the nonlinear crystal results in two SPDCs and one SFG to generate the triphoton state. The generated beams, registered by point photodetectors, may pass through some linear, passive optical systems (OS) placed between the crystal and the detectors.

Using Glauber's theory, the averaged triphoton coincidence counting rate is defined by

$$R_3=\lim_{T\to\infty}\frac{1}{T}\int_0^T dt_1\int_0^T dt_2\int_0^T dt_3$$
$$\times\langle\Psi|E_1^{(-)}E_2^{(-)}E_3^{(-)}E_3^{(+)}E_2^{(+)}E_1^{(+)}|\Psi\rangle, \quad (10)$$

the two~photon coincidence counting rate is

$$R_2=\lim_{T\to\infty}\frac{1}{T}\int_0^T dt_1\int_0^T dt_2\langle\Psi|E_1^{(-)}E_2^{(-)}E_2^{(+)}E_1^{(+)}|\Psi\rangle, \quad (11)$$

and the singles counting rate at detector D1 is given by

$$R_1=\lim_{T\to\infty}\frac{1}{T}\int_0^T dt_1\langle\Psi|E_1^{(-)}E_1^{(+)}|\Psi\rangle. \quad (12)$$

$E_j^{(+)}$ is the positive frequency part of the electromagnetic field evaluated at the jth detector's spatial coordinate $\vec{r}_j=\vec{\rho}_j+z_j\hat{z}$ and trigger time t_j. The propagation of these free-space electromagnetic fields is governed by the transformation

$$E_j^{(+)}=\sum_{\vec{k}_j}E_j e^{-i\omega_j t_j}g_j(\vec{k}_j,\vec{r}_j)a(\vec{k}_j), \quad (13)$$

where $E_j=i\sqrt{\hbar\omega_j/2\varepsilon_0 V}$. The function g_j is the Green's function which depends on the transverse coordinate of the jth

detector, $\vec{\rho}_j$, and the distance from the output surface of the crystal to the plane of the detector, z_j.

By using Eq. (3), the sixth-order field correlation function becomes

$$G^{(3)} = \langle\Psi|E_1^{(-)}E_2^{(-)}E_3^{(-)}E_3^{(+)}E_2^{(+)}E_1^{(+)}|\Psi\rangle = |\langle 0|E_3^{(+)}E_2^{(+)}E_1^{(+)}|\Psi\rangle|^2 = |A_3|^2, \tag{14}$$

where A_3 is called the triphoton amplitude. Similarly, the fourth-order field correlation function becomes

$$G^{(2)} = \langle\Psi|E_1^{(-)}E_2^{(-)}E_2^{(+)}E_1^{(+)}|\Psi\rangle = \sum_{\vec{k}_3} |\langle 0|a(\vec{k}_3)E_2^{(+)}E_1^{(+)}|\Psi\rangle|^2 = \sum_{\vec{k}_3} |A_2|^2. \tag{15}$$

The second-order field correlation function may be written as

$$G^{(1)} = \langle\Psi|E_1^{(-)}E_1^{(+)}|\Psi\rangle = \sum_{\vec{k}_2}\sum_{\vec{k}_3} |\langle 0|a(\vec{k}_3)a(\vec{k}_2)E_1^{(+)}|\Psi\rangle|^2 = \sum_{\vec{k}_2}\sum_{\vec{k}_3} |A_1|^2. \tag{16}$$

First, let us look at the triphoton coincidence counts. For the experiment illustrated in Fig. 1(a), suppose that the two signal beams produced from SPDCs are sent to detectors D1 and D2 while the up-converted photon is recorded by detector D3. By using Eqs. (3), (13), and (14), we have

$$A_3 = A_3^0 \sum_{\vec{k}_{s1}}\sum_{\vec{k}_{s2}}\sum_{\vec{k}_u} e^{-i(\omega_{s1}t_1+\omega_{s2}t_2+\omega_u t_3)} g_1(\vec{k}_{s1},\vec{r}_1) g_2(\vec{k}_{s2},\vec{r}_2) \times g_3(\vec{k}_u,\vec{r}_3) F(\vec{k}_{s1},\vec{k}_{s2},\vec{k}_u), \tag{17}$$

where $A_3^0 = \beta E_1 E_2 E_3$. Next, we perform the two~photon coincidence counts in the triphoton entangled state. As an example, we examine the case that only one of the down-converted photons trigger detector D1 and the up-converted photon triggers D2. Other possible arrangements are left as an exercise. By using Eqs. (3), (13), and (15), we have

$$A_2 = A_2^0 \sum_{\vec{k}_{s2}}\sum_{\vec{k}_u} e^{-i(\omega_{s2}t_1+\omega_u t_2)} g_1(\vec{k}_{s2},\vec{r}_1) g_2(\vec{k}_u,\vec{r}_2) F(\vec{k}_{s1},\vec{k}_{s2},\vec{k}_u), \tag{18}$$

where $A_2^0 = \beta E_1 E_2$. For the single-photon detection, we consider one case that the detector D1 detects the up-converted photons. By using Eqs. (3), (13), and (16), we have

$$A_1 = A_1^0 \sum_{\vec{k}_u} e^{-i\omega_u t_1} g_1(\vec{k}_u,\vec{r}_1) F(\vec{k}_{s1},\vec{k}_{s2},\vec{k}_u), \tag{19}$$

where $A_1^0 = \beta E_1$. Equations (17)–(19) clearly show how the counting rates are determined by the classical optical transfer functions g and the triphoton spectral function F. In the biphoton optics of SPDC, based on the properties of Green's function, Klyshko gave an intuitive pictorial description, named advanced-wave model [19], to interpret the two-photon phenomena. One of the photons is created at one detector, propagates back to the source where it becomes the second photon, and then propagates forward in time to the second detector. For the triphoton geometrical optics discussed here, this intuitive advanced-wave picture is still applicable but with some modifications, as we shall see in the following sections.

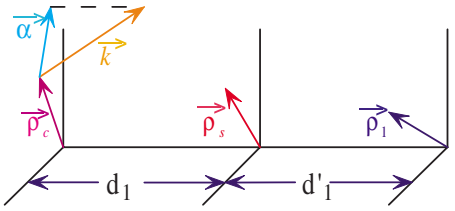

FIG. 2. (Color online) The output surface of the crystal forms the $\vec{\rho}_c$ plane, the optical system specified by an aperture function $s_1(\vec{\rho}_s)$ is in the s plane, and photo-detector D1 is placed in the $\vec{\rho}_1$ plane. The distance between the aperture and output surface of the crystal is d_1 and d_1' is the distance between the aperture and detector planes. $\vec{\alpha}$ is the transverse component of the wave vector $\vec{k}$.

In the following discussion, for simplicity, it is always assumed that the pump is a monochromatic plane wave traveling along the z axis with a cross section large enough so that the transverse detuning function H can be taken to be a δ function: $H(\vec{\alpha}+\vec{\alpha}') = \delta_{\vec{\alpha}+\vec{\alpha}'}$. In the whole process, the energy conservation $\Omega_{s1}+\Omega_{s2}+\Omega_u = 2\Omega_p$ is always well-satisfied.

A. Single-photon counting rate

First, let us look at the single-photon counting rate for the experiment drawn in Fig. 1(a). The result showed that the singles counting rate has no structure in experiments. Considering the case of up-converted photons triggering detector D1, it is not difficult to show using Eqs. (12) and (16) that the singles counting rate is independent of time, and may be written using Eqs. (4), (9), and (A9) as

$$R_1 = R_1^0 \int d^2\alpha_{s1} \int d^2\alpha_{s2} \left| S_1\left(-\vec{\alpha}_{s1}-\vec{\alpha}_{s2}-\frac{\omega_u}{cd_1'}\vec{\rho}_1, \frac{\omega_u}{cd_1'}\right)\right|^2 \times \int d\nu_1 \int d\nu_2 \left[\operatorname{sinc}\left(\frac{\nu_1 D_{11} L}{2} + \frac{\alpha_{s1}^2 L}{2K_1}\right) \times \operatorname{sinc}\left(\frac{\nu_2 D_{22} L}{2} + \frac{\alpha_{s2}^2 L}{2K_2}\right) \operatorname{sinc}\left[\frac{(\nu_1 D_{13}+\nu_2 D_{23})L}{2} + \frac{(\vec{\alpha}_{s1}+\vec{\alpha}_{s2})^2 L}{2K_u} - \frac{\alpha_{s1}^2 L}{2K_{i1}} - \frac{\alpha_{s2}^2 L}{2K_{i2}} \right] \right]^2, \tag{20}$$

where R_1^0 has absorbed all the slowly varying constants, and S_1 is the Fourier transform of the aperture function modeling the optical system in front of detector D1 and is defined in Eq. (A9). In Eq. (20), d_1' is the distance between the aperture plane and the detector, see Fig. 2, $1/K_1 = 1/K_{s1} + 1/K_{i1}$ and $1/K_2 = 1/K_{s2} + 1/K_{i2}$. In the derivation of Eq. (20), we have converted the sum into the usual integral by $[\Sigma_{\vec{k}} = V/(2\pi)^3 \int d^2\alpha \int d\nu/u]$. The integrals over ν_j may be determined by the form of filtering used. In experiments, the fil-

tering may be done directly by placing a filter in the beam or indirectly by using a small pinhole to limit the range of $\vec{\alpha}_j$ that enters the detector. If the bandwidth of the filter is large compared to the natural spectral width of triphoton, the integrals over the frequencies will give a constant and the integrals over the transverse components of the wave numbers will also give a constant for all $\vec{\rho}_1$ in the paraxial region. If we take the optical system to be a lens of focal length f with aperture radius r_a, and the detector D1 is placed in the focal plane of the lens, S_1 turns to be the Fourier transform of the aperture (A9). The singles counting rate simply becomes

$$R_1 = R_1^0 \int d^2\alpha_{s1} \int d^2\alpha_{s2} \left[\frac{J_1(|\vec{\alpha}_{s1}+\vec{\alpha}_{s2}|r_a)}{|\vec{\alpha}_{s1}+\vec{\alpha}_{s2}|r_a} \right]^2 \int d\nu_1 \int d\nu_2 \times \left[\mathrm{sinc}\left(\frac{\nu_1 D_{11} L}{2} + \frac{\alpha_{s1}^2 L}{2K_1} \right) \times \mathrm{sinc}\left(\frac{\nu_2 D_{22} L}{2} + \frac{\alpha_{s2}^2 L}{2K_2} \right) \mathrm{sinc}\left[\frac{(\nu_1 D_{13} + \nu_2 D_{23}) L}{2} + \frac{(\vec{\alpha}_{s1}+\vec{\alpha}_{s2})^2 L}{2K_u} - \frac{\alpha_{s1}^2 L}{2K_{i1}} - \frac{\alpha_{s2}^2 L}{2K_{i2}} \right] \right]^2, \tag{21}$$

where $J_1(x)$ is the Bessel function of first kind. If the aperture is of the order of tenths of millimeters, then the range of $\vec{\alpha}$ is determined by the Bessel function to be a few mm^{-1}. Over this range, the diffraction effects of a single slit cannot be observed. In addition, if the slit is replaced by a double slit, the Young's interference fringes will be washed out.

B. Two~photon coincidence counting rate

Next, we consider the two~photon coincidence counting rate in a triphoton entangled state for the experiment shown in Fig. 1(a). As an example, we look at the case that only one optical system is placed in one of the down-converted beams (e.g., the $s2$ beam) which is detected by detector D1 while detector D2 registers the up-conversion photons. In this case, Eq. (18) becomes

$$A_2 = A_2^0 \sum_{\vec{k}_{s2}} e^{-i(\omega_{s2} T_1 + \omega_u T_2)} \psi\left(\vec{\rho}_1, \frac{\omega_{s2}}{c d_1'} \right) \times S_1\left(\vec{\alpha}_{s2} - \frac{\omega_{s2}}{c d_1'} \vec{\rho}_1, \frac{\omega_{s2}}{c d_1'} \right) \psi\left(\vec{\alpha}_{s2}, -\frac{c d_1}{\omega_{s2}} \right) \times \psi\left(-\vec{\alpha}_{s1} - \vec{\alpha}_{s2}, -\frac{c z_2}{\omega_u} \right) \times e^{-i(\vec{\alpha}_{s1}+\vec{\alpha}_{s2})\cdot\vec{\rho}_2} \Phi(\delta k_{\mathrm{I}} L) \Phi(\delta k_{\mathrm{II}} L) \Phi(\delta k_{\mathrm{III}} L), \tag{22}$$

where $T_j = t_j - z_j/c$ for $j=1,2$. The function $\psi(\vec{r},x)$ is defined in Appendix A and takes the Gaussian form. Next, we denote $\tau = T_1 - T_2$ as the timing difference between two detectors D1 and D2 and convert the sum into the usual integrals. All the slowly varying terms and phase factors are again grouped into A_2^0. In the paraxial approximation, Eq. (22) can be further written as

$$A_2 = A_2^0 \int d^2\alpha_{s2} \psi\left(\vec{\alpha}_{s2}, -\frac{c d_1}{\omega_{s2}} \right) S_1\left(\vec{\alpha}_{s2} - \frac{\omega_{s2}}{c d_1'} \vec{\rho}_1, \frac{\omega_{s2}}{c d_1'} \right) \times \psi\left(-\vec{\alpha}_{s1} - \vec{\alpha}_{s2}, -\frac{c z_2}{\omega_u} \right) e^{-i(\vec{\alpha}_{s1}+\vec{\alpha}_{s2})\cdot\vec{\rho}_2} \int d\nu_2 \times e^{-i\nu_2\tau} \mathrm{sinc}\left(\frac{\nu_2 D_{22} L}{2} + \frac{\alpha_{s2}^2 L}{2K_2} \right) \times \mathrm{sinc}\left[\frac{(\nu_1 D_{13} + \nu_2 D_{23}) L}{2} + \frac{(\vec{\alpha}_{s1}+\vec{\alpha}_{s2})^2 L}{2K_u} - \frac{\alpha_{s1}^2 L}{2K_{i1}} - \frac{\alpha_{s2}^2 L}{2K_{i2}} \right]. \tag{23}$$

The integral over ν_2 can be evaluated using

$$\nu_{02} = \frac{\alpha_{s2}^2}{D_{22} K_2}, \quad \nu_{03} = \frac{1}{D_{23}} \left[\nu_1 D_{13} - \frac{\alpha_{s1}^2}{K_{i1}} - \frac{\alpha_{s2}^2}{K_{i2}} + \frac{(\vec{\alpha}_{s1}+\vec{\alpha}_{s2})^2}{K_u} \right]. \tag{24}$$

For a filter with broad bandwidth, the integral over ν_2 is simply the Fourier transform of the product of two sinc functions, which leads to

$$\int d\nu_2 e^{-i\nu_2\tau} \mathrm{sinc}\left[\frac{(\nu_2 + \nu_{02}) D_{22} L}{2} \right] \mathrm{sinc}\left[\frac{(\nu_2 + \nu_{03}) D_{23} L}{2} \right] = \wedge(\tau, \nu_{02}, \nu_{03}, D_{22}L, D_{23}L; \nu_2), \tag{25}$$

where the function $\wedge$ is provided in Appendix B. Equation (25) shows how the frequency and wave number phase matching interlock the spatial and temporal coherence. In general, the spatial and temporal effects cannot be separated in discussing the two-photon (and multiphoton) transverse correlation. For simplicity, in the following discussions we ignore the transverse components of wave vectors in the longitudinal phase matching. This approximation may allow us to deal with the transverse and longitudinal components of wave vectors in the two~photon (and three-photon) coincidence counting rate separately. So, Eq. (23) now can be written as

$$A_2 = A_2^0 A_2^{tr} \times A_2^{lg}, \tag{26}$$

where the subscript tr means the transverse part and lg the longitudinal part.

Using Eq. (A9) and regrouping the constants and phase factors into A_2^0, we find

$$A_2^{tr} = \int d^2\rho_s s_1(\vec{\rho}_s) e^{-i\vec{\rho}_s\cdot\vec{\alpha}_0} \psi\left(\vec{\rho}_s, \frac{\omega_{s2}}{c d_{\mathrm{eff}}^{(2)}} \right), \tag{27}$$

where

$$\vec{\alpha}_0 = \frac{\omega_{s2}}{c d_1'} \vec{\rho}_1 + \frac{1}{c\left(\frac{d_1}{\omega_{s2}} + \frac{z_2}{\omega_u} \right)} \vec{\rho}_2 + \frac{\frac{z_2}{\omega_u}}{\frac{d_1}{\omega_{s2}} + \frac{z_2}{\omega_u}} \vec{\alpha}_{s1},$$

$$\frac{1}{d_{\text{eff}}^{(2)}} = \frac{1}{d_1'} + \frac{1}{d_1 + \left(\frac{\omega_{s2}}{\omega_u}\right) z_2}. \tag{28}$$

On the one hand, in the far-field Fraunhofer approximation, the ψ's in Eq. (27) goes to unity and it leads to a Fourier transform of the aperture function. On the other hand, in standard optics it is known that the Fresnel phase factor can be removed by placing a converging lens of focal length f in the aperture plane and placing the detectors in the appropriate optical planes. In other words, set $d_{\text{eff}}^{(2)}=f$, so that A_2^{tr} is proportional to the Fourier transform of $t(\vec{\rho}_s)$, which is the transmittance function of the aperture as discussed in Appendix A. That is, we choose

$$\frac{1}{d_1'} + \frac{1}{d_1 + (\omega_{s2}/\omega_u) z_2} = \frac{1}{f}. \tag{29}$$

Equation (29) is the same as that for the SPDC source [see Eq. (70) in Ref. [10]] and it has the form of GTLE relating the object and image plane to the focal length of a lens in geometrical optics. As seen in Eq. (29), $d_1+(\omega_{s2}/\omega_u)z_2$ is the distance from the lens to the crystal plus the distance from the crystal to detector D2 weighted by the ratio of the free-space wavelengths. The magnification of the inverted image is $f/(d_1'-f)$. The image which appears in the coincidence counting rate is, using Eqs. (11), (15), and (27),

$$R_2^{tr} = \int d^2\alpha_{s1} \left| S_1\left(\vec{\alpha}_0, \frac{\omega_{s2}}{cf}\right)\right|^2. \tag{30}$$

Note that this image is not localized at either detector. The difference between this result and Eq. (71) in Ref. [10] is that the image becomes blurred because of tracing the transverse component of the wave vector of the remaining down-converted $s1$ beam. The relationship between the object and the image can be obtained by completing the integration in Eq. (27) over the effective area of the lens,

$$\int d^2\rho_s e^{-i\vec{\rho}_s\cdot\vec{\alpha}_0} \simeq \delta\left(\frac{\vec{\rho}_1}{d_1'} + \frac{\vec{\rho}_2}{d_1 + (\omega_{s2}/\omega_u) z_2} + \frac{(z_2/\omega_u) c\vec{\alpha}_{s1}}{d_1 + (\omega_{s2}/\omega_u) z_2}\right),$$

where Eq. (28) is applied. In the derivation of the above relationship, we have assumed an infinite-size lens. As we see, the point-point relationship between the object ($\vec{\rho}_1$) and image ($\vec{\rho}_2$) is manifested by the remaining transverse modes in the untouched $s1$ beam. The magnification of the inverted image is $[d_1+(\omega_{s2}/\omega_u)z_2]/d_1'$. If the lens has a finite size, the above integral will yield a function of $J_1(x)/x$, where $J_1(x)$ is the Bessel function of first kind. From Eq. (30), it is obvious that the more transverse modes generated in the parametric processes, the worse the quality of the image. In this two-photon imaging, the advanced-wave model is valid and provides an intuitive picture to understand the relation between the object and the image. For other possible experimental arrangements of placing the optical system, one may find similar results as Eqs. (27)–(30).

C. Triphoton coincidence counting rate

We now turn to study the triphoton coincidence counting rate for the experiment diagramed in Fig. 1(a). Here we will examine two instances. In the first one, we only place one OS in one of the down-converted beams. In the second example, one OS is placed in the up-converted beam and the other one is put in one of the down-converted beams. Other possible arrangements may be analyzed using the same procedure and we leave them as exercises. So, let us start with the first case that the OS is placed in one of the down-converted beams (e.g., $s1$ beam). Under this experimental setup, using the results given in Appendix A, the triphoton amplitude (17) becomes

$$\begin{aligned} A_3 = A_3^0 \sum_{\vec{k}_{s1}} \sum_{\vec{k}_{s2}} & e^{-i(\omega_{s1}T_1+\omega_{s2}T_2+\omega_u T_3)} \psi\left(\vec{\rho}_1, \frac{\omega_{s1}}{cd_1'}\right) \\ & \times S_1\left(\vec{\alpha}_{s1} - \frac{\omega_{s1}}{cd_1'}\vec{\rho}_o, \frac{\omega_{s1}}{cd_1'}\right) \psi\left(\vec{\alpha}_{s1}, -\frac{cd_1}{\omega_{s1}}\right) \psi\left(\vec{\alpha}_{s2}, -\frac{cz_2}{\omega_{s2}}\right) \\ & \times \psi\left(-\vec{\alpha}_{s1} - \vec{\alpha}_{s2}, -\frac{cz_3}{\omega_u}\right) \\ & \times e^{i\vec{\alpha}_{s2}\cdot\vec{\rho}_2} e^{-i(\vec{\alpha}_{s1}+\vec{\alpha}_{s2})\cdot\vec{\rho}_3} \Phi(\delta k_{\text{I}} L)\Phi(\delta k_{\text{II}} L)\Phi(\delta k_{\text{III}} L). \end{aligned} \tag{31}$$

Again, all the slowly varying terms and phase factors are absorbed into A_3^0. Under the same assumption that the natural width of triphoton does not affect the transverse correlations, we write the triphoton amplitude as the product of transverse and longitudinal parts separately, i.e.,

$$A_3 = A_3^0 A_3^{tr} \times A_3^{lg}, \tag{32}$$

where the transverse part is given by

$$A_3^{tr} = \int d^2\rho_s s_1(\vec{\rho}_s) e^{-i\vec{\rho}_s\cdot\vec{\alpha}_{03}} \psi\left(\vec{\rho}_s, \frac{\omega_{s1}}{cd_{\text{eff}}^{(31)}}\right), \tag{33}$$

where

$$\vec{\alpha}_{03} = \frac{\omega_{s1}}{cd_1'}\vec{\rho}_o + \frac{\omega_{s1}}{cd_1}\frac{\frac{\omega_{s2}}{z_2}\vec{\rho}_2 + \frac{\omega_u}{z_3}\vec{\rho}_3}{\frac{\omega_{s1}}{d_1} + \frac{\omega_{s2}}{z_2} + \frac{\omega_u}{z_3}}, \quad \frac{1}{d_{\text{eff}}^{(31)}} = \frac{1}{d_1'} + \frac{1}{d_1 + \mathcal{L}^{(31)}}, \tag{34}$$

and

$$\frac{\omega_{s1}}{\mathcal{L}^{(31)}} = \frac{\omega_{s2}}{z_2} + \frac{\omega_u}{z_3}. \tag{35}$$

In the far-field approximation, the ψ's in Eq. (33) become unity and it turns out to be the Fourier transform of the aperture. For the quantum imaging, we may remove the Fresnel phase factor by placing a converging lens of focal length f in the aperture plane, i.e., setting $d_{\text{eff}}^{(31)}=f$, so that A_3^{tr} is a function of the Fourier transform of $t(\vec{\rho}_s)$. That is

$$\frac{1}{d_1'} + \frac{1}{d_1 + \mathcal{L}^{(31)}} = \frac{1}{f}. \tag{36}$$

It is obvious that Eq. (36) is the GTLE form. Comparing with the biphoton geometrical optics (29), one difference is the distance between the lens and imaging plane. From Eq. (36), this distance becomes the distances from the lens to the crystal (d_1) plus the effective length $\mathcal{L}^{(31)}$ from the crystal to the imaging plane. The effective length $\mathcal{L}^{(31)}$ [Eq. (35)] is a

parallel combination of distances between the crystal and two detectors weighted by wavelengths, which behaves as the parallel combination of resistors in the electromagnetism theory. The positions of two remaining detectors are not unique, which is easy to verify from Eq. (35). The image shown in the triphoton coincidence counting rate is

$$R_3^{tr} = \left| S_1\left(\vec{\alpha}_{03}, \frac{\omega_{s1}}{cf}\right)\right|^2. \tag{37}$$

Whether the relation between the object and the image is a point-point correspondence can be deduced from Eq. (33) with the help of Eqs. (34) and (35). Performing the integral over the lens with an infinite size in Eq. (33) then gives

$$\int d^2\rho_s e^{-i\vec{\rho}_s\cdot\vec{\alpha}_{02}} \simeq \delta\left(\frac{\omega_{s1}\vec{\rho}_o}{d_1'} + \frac{\frac{\omega_{s2}}{z_2}\vec{\rho}_2 + \frac{\omega_u}{z_3}\vec{\rho}_3}{1 + d_1/\mathcal{L}^{(31)}}\right).$$

As seen from the above result, the point-point correspondence between the object ($\vec{\rho}_o$) and the image ($\vec{\rho}_2$, $\vec{\rho}_3$), is well-defined in the case discussed in this section. There are two types of operations to perform the triphoton coincidences. One way is to fix one detector, say D2, and only move the other detector D3. The magnification of the inverted image is given by $(\omega_{31}/\omega_u)(1+d_1/\mathcal{L}^{(31)})(z_3/d_1')$. The other case is to move both detectors D2 and D3 together. In such a case, the magnification of the inverted image is given by $(d_1+\mathcal{L}^{(31)})/d_1'$. The difference of the magnifications for these two cases is represented by the ratio $(\omega_{31}z_3)/(\omega_u d_1)$. Of course, the finite-size lens will give a function of $J_1(x)/x$. Making a comparison between Eqs. (37) and (30), one may find that in the two~photon coincidences, the blurred image is due to tracing the remaining freedom in $s1$ photons; while in the triphoton coincidence counting rate, the image has a better resolution and Eq. (37) exactly has the same consequence as Eq. (71) in Ref. [10]. The magnification of the inverted image is $f/(d_1'-f)$. Note again that the image is not localized at either detector. Klyshko's advanced-wave model now should be interpreted as the *effective* two-photon picture, in which one of the photons is created at detector D1, and propagates back to the source where it becomes the *second* photon. Then this photon propagates forward in time to the *effective second* detector which is located in the effective length $\mathcal{L}^{(31)}$ away from the crystal.

One may wonder if one object with two lenses is placed in the system, how many images can be observed in the coincidences, one or two? The answer is generally two obscure images may be obtained in the imaging planes. However, by carefully choosing the experimental parameters, one may see two *good* images with different magnifications, to some extent. The reason is analyzed in the following example.

In the second example, we will look at the case where one OS is placed in one of the down-converted beams (e.g., the $s1$ beam) and the second OS is in the up-converted beam. The triphoton amplitude (17) now turns to be

$$\begin{aligned} A_{32} = A_{32}^0 \sum_{\vec{k}_{s1}} \sum_{\vec{k}_{s2}} & e^{-i(\omega_{s1}T_1+\omega_{s2}T_3+\omega_u T_2)} S_1\left(\vec{\alpha}_{s1} - \frac{\omega_{s1}}{cd_1'}\vec{\rho}_1, \frac{\omega_{s1}}{cd_1'}\right) \\ & \times \psi\left(\vec{\alpha}_{s1}, -\frac{cd_1}{\omega_{s1}}\right)\psi\left(\vec{\alpha}_{s2}, -\frac{cz_3}{\omega_{s2}}\right) S_2 \\ & \times \left(-\vec{\alpha}_{s1} - \vec{\alpha}_{s2} - \frac{\omega_u}{cd_2'}\vec{\rho}_2, \frac{\omega_u}{cd_2'}\right)\psi \\ & \times \left(-\vec{\alpha}_{s1} - \vec{\alpha}_{s2}, -\frac{cd_2}{\omega_u}\right) \\ & \times e^{i\vec{\alpha}_{s2}\cdot\vec{\rho}_3}\Phi(\delta k_{\mathrm{I}}L)\Phi(\delta k_{\mathrm{II}}L)\Phi(\delta k_{\mathrm{III}}L). \end{aligned} \tag{38}$$

All the slow constants and phase factors are grouped into A_{32}^0. Similarly, separate the triphoton amplitude (38) into transverse and longitudinal parts,

$$A_{32} = A_{31}^0 A_{32}^{tr} \times A_{32}^{lg}. \tag{39}$$

After some algebra, the transverse part is given by

$$\begin{aligned} A_{32}^{tr} = \int d^2\rho_{s1} \int d^2\rho_{s2} & s_1(\vec{\rho}_{s1}) s_2(\vec{\rho}_{s2}) \\ & \times e^{-i\vec{\rho}_{s1}\cdot\vec{\alpha}_1} e^{-i\vec{\rho}_{s2}\cdot\vec{\alpha}_2} e^{-i\vec{\rho}_{s1}\cdot\vec{\rho}_{s2}/l^2} \psi\left(\vec{\rho}_{s1}, \frac{\omega_{s1}}{cd_{s1}}\right) \\ & \times \psi\left(\vec{\rho}_{s2}, \frac{\omega_u}{cd_{s2}}\right), \end{aligned} \tag{40}$$

where

$$\vec{\alpha}_1 = \frac{\omega_{s1}}{cd_1'}\vec{\rho}_1 + \frac{\omega_{s1}}{cd_1}\frac{\frac{\omega_{s2}}{z_3}\vec{\rho}_3}{\frac{\omega_{s1}}{d_1} + \frac{\omega_{s2}}{z_3} + \frac{\omega_u}{d_2}},$$

$$\vec{\alpha}_2 = \frac{\omega_u}{cd_2'}\vec{\rho}_2 + \frac{\omega_u}{cd_2}\frac{\frac{\omega_{s2}}{z_3}\vec{\rho}_3}{\frac{\omega_{s1}}{d_1} + \frac{\omega_{s2}}{z_3} + \frac{\omega_u}{d_2}},$$

$$\frac{1}{l^2} = \frac{\frac{\omega_{s1}\omega_u}{cd_1d_2}}{\frac{\omega_{s1}}{d_1} + \frac{\omega_{s2}}{z_3} + \frac{\omega_u}{d_2}}; \quad \frac{1}{d_{s1}} = \frac{1}{d_1'} + \frac{1}{d_1 + \mathcal{L}_1^{(32)}}, \quad \frac{1}{d_{s2}} = \frac{1}{d_2'} + \frac{1}{d_2 + \mathcal{L}_2^{(32)}}; \tag{41}$$

and

$$\frac{\omega_{s1}}{\mathcal{L}_1^{(32)}} = \frac{\omega_u}{d_2} + \frac{\omega_{s2}}{z_3}, \quad \frac{\omega_u}{\mathcal{L}_2^{(32)}} = \frac{\omega_{s1}}{d_1} + \frac{\omega_{s2}}{z_3}. \tag{42}$$

Using the same analog, in the far-field Fraunhofer approximation, the ψ's in Eq. (40) go to unity and they become a joint Fourier transform of two apertures. This joint Fourier transform of two apertures generally cannot be separated because of the third crossed phase factor $e^{-i\vec{\rho}_{s1}\cdot\vec{\rho}_{s2}/l^2}$ in Eq. (40). The effect of this crossed phase term will be further discussed in the next section by considering the ghost interference-diffraction experiments, using double slits as apertures. In order to look at the ghost imaging process, we remove the Fresnel phase factors by placing one lens of focal

length f_1 in the aperture plane 1 and another lens of focal length f_2 in the aperture plane 2, i.e., setting $f_1=d_{s1}$ and $f_2=d_{s2}$, then A_{32}^{tr} is proportional to the joint Fourier transform of the transmittance function of two lenses $t(\vec{\rho}_{s1})$ and $t(\vec{\rho}_{s2})$. To satisfy the GTLEs, the condition $(\omega_{s1}f_1d_1'd_2)/(\omega_u f_2 d_2' d_1)=(f_1d_1'+f_1d_1-d_1'd_1)/(f_2d_2'+f_2d_2-d_2'd_2)$ should be satisfied. There is one special case to get rid of the Fresnel phase factors, in which only one lens of focal length f is needed if we require the relationship $z_3/\omega_{s2}=-(d_1-d_2)/(\omega_u-\omega_{s2})$. After setting $f_1=d_{s1}$ and $f_2=d_{s2}$, the transverse part of the triphoton coincidence counting rate becomes

$$R_{32}^{tr}=\left|\mathcal{S}\left(\vec{\alpha}_1,\ \frac{\omega_{s1}}{cf_1};\ \vec{\alpha}_2,\ \frac{\omega_u}{cf_2}\right)\right|^2. \tag{43}$$

In Eq. (43) we have defined the two-image-amplitude Fourier transform, which is

$$\mathcal{S}\left(\vec{\alpha}_1,\ \frac{\omega_{s1}}{cf_1};\ \vec{\alpha}_2,\ \frac{\omega_u}{cf_2}\right)=\int d^2\rho_{s1}\int d^2\rho_{s2}t_1(\vec{\rho}_{s1})t_2(\vec{\rho}_{s2})e^{-i\vec{\rho}_{s1}\cdot\vec{\alpha}_1}e^{-i\vec{\rho}_{s2}\cdot\vec{\alpha}_2}e^{-i\vec{\rho}_{s1}\cdot\vec{\rho}_{s2}/l^2}. \tag{44}$$

The relationship between two objects $(\vec{\rho}_1,\ \vec{\rho}_2)$ and two images $(\vec{\rho}_3)$ can be derived from Eq. (44) as follows:

$$\int d^2\rho_{s1}\int d^2\rho_{s2}e^{-i\vec{\rho}_{s1}\cdot\vec{\alpha}_1}e^{-i\vec{\rho}_{s2}\cdot\vec{\alpha}_2}e^{-i\vec{\rho}_{s1}\cdot\vec{\rho}_{s2}/l^2}\simeq l^4e^{il^2\vec{\alpha}_1\cdot\vec{\alpha}_2},$$

where two lenses are assumed to have the infinite size. In general, the above result states that the point-point correspondence between object and image is not well-defined in such a case, even though the GTLEs are satisfied. Alternatively, the general conclusion about the resolution for the imaging could not be reached. The physics can be simply argued as since both images are related with detector D3, one image is washed out by the other image. However, there is a case, if $z_3\ll d_{1,2}$, that the above result may be approximated as two δ functions, i.e., $\delta\left(\frac{\vec{\rho}_1}{d_1'}+\frac{\omega_{s2}\mathcal{L}_1^{(32)}}{\omega_{s1}z_3}\frac{\vec{\rho}_3}{d_1+\mathcal{L}_1^{(32)}}\right)\delta\left(\frac{\vec{\rho}_2}{d_2'}+\frac{\omega_{s2}\mathcal{L}_2^{(32)}}{\omega_u z_3}\frac{\vec{\rho}_3}{d_2+\mathcal{L}_2^{(32)}}\right)$. It is clear that under such a situation, the triphoton imaging is reduced to two sets of independent two-photon imaging processes and the point-point relation between object and image is recovered, to some extent. Let us go back to Eq. (42). Now it turns out to be GTLEs which determine the positions of two imaging planes. However, from the two-image-amplitude Fourier transform (44), the point-point correspondence for the imaging process now spreads to become the point-plane correspondence due to the crossed phase term. This means that in the imaging planes, generally, two images get blurred and share the information of both objects. To get high-quality images, one has to decrease the function of the crossed phase term in Eq. (44) by setting $z_3\ll d_{1,2}$, as discussed above. This will lead to two approximately independent images. Therefore the crossed phase term in Eq. (44) plays an important role in determining the imaging qualities. As stated in Eq. (44), the two images are generally not independent and they are correlated. To further confirm this point, one may go back to examine Eq. (42). In Eq. (42), the effective lengths $\mathcal{L}_{1,2}^{(32)}$ are the parallel combination of distances from the imaging lens to crystal and from the crystal to detector D3 weighted by wavelengths. By setting $z_3\ll d_{1,2}$, the effective lengths $\mathcal{L}_{1,2}^{(32)}$ are approximated as only a function of z_3. The triphoton coincidence counts now can be decoupled into two two-photon coincidence counts. When $z_3/\omega_{s2}=-(d_1-d_2)/(\omega_u-\omega_{s2})$, two images share the same imaging plane but may possess different magnifications.

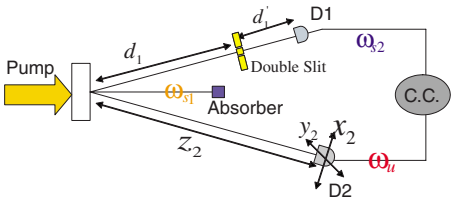

FIG. 3. (Color online) Two-photon ghost interference-diffraction experiment setup with one double slit. The double slit is inserted in the ω_{s2} beam and the detector D2 is scanned in its transverse plane. The ω_{s1} beam is absorbed by an absorber. The parameters of the double slit are $a=0.5$ mm, $b=0.1$ mm, and $\ell=1$ cm.

IV. GHOST INTERFERENCE-DIFFRACTION EXPERIMENTS OF DOUBLE SLITS

Like entangled-photon image transfer, the correlated-photon transverse interference is a manifestation of angular (transverse wave vectors) correlation of entangled states. In analogy with the usual optical terminology, the imaging transfer belongs to geometrical triphotonics, while the interference and diffraction belong to physical triphotonics. In this section, let us consider a triphoton analog of Young's interference experiments. In Young's experiment, the slits having width b separated by a distance a between their centers are illuminated by a light source. The aperture function of the double slit takes the form

$$s(\vec{\rho})=\left[\mathrm{rect}\left(\frac{x+a/2}{b}\right)+\mathrm{rect}\left(\frac{x-a/2}{b}\right)\right]\mathrm{rect}\left(\frac{y}{\ell}\right), \tag{45}$$

where ℓ is the length of the slits. If the double slit is illuminated coherently, this requires that the wave-vector spectrum of the source is much narrower than $2\pi/a$. Interference fringes can be observed on a screen at a distance z behind the slits. In the following, we will devise a triphoton analog of the Young's experiments with the coincidence counting measurement as discussed in Sec. III.

To connect with the biphoton ghost interference-diffraction experiment done in SPDC [11], we revisit this experiment replaced with a triphoton source (see Fig. 3). The ghost interference-diffraction pattern which is obtained in the two~photon coincidence detection now becomes

$$R_2^{tr}(x_2,y_2)=\int d\alpha_{s1,x}\cos^2\left(\frac{a\alpha_{01,x}}{2}\right)\mathrm{sinc}^2\left(\frac{b\alpha_{01,x}}{2}\right)\times\int d\alpha_{s1,y}\ \mathrm{sinc}^2\left(\frac{\ell\alpha_{01,y}}{2}\right), \tag{46}$$

where we have decomposed $\vec{\alpha}_{01}$ and $\vec{\alpha}_{s1}$ in the (x,y) plane

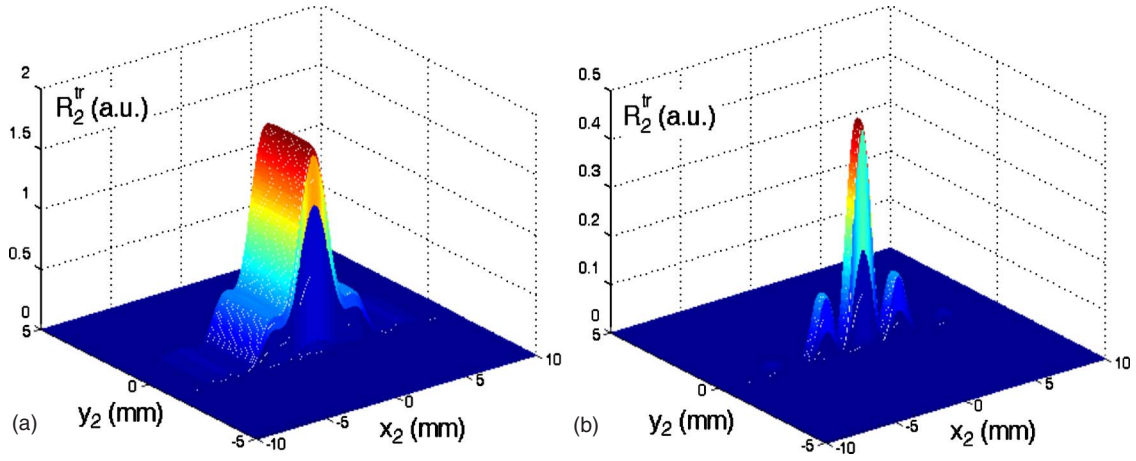

FIG. 4. (Color online) Ghost interference-diffraction pattern of a double slit in a two~photon coincidence counting measurement by using a triphoton entanglement source: (a) with many transverse modes in the nondetected $s1$ beam; and (b) with few transverse modes. The parameters were chosen as $d_1'=1$ m, $d_1=0.3$ m, and $z_2=1.8$ m.

and ignored the constants. According to the advanced-wave picture, the interpretation of Eq. (46) is to think of detector D1 as an advanced-wave source placed at a distance d_1' from the double slit and scanning transverse coordinates (x_2,y_2) of detector D2 which is at $d_1+(\omega_{s2}/\omega_u)z_2$ away from the double slit where $[d_1+(\omega_{s2}/\omega_u)z_2]\gg a^2/\lambda_{s2}$ and $[d_1+(\omega_{s2}/\omega_u)z_2]\gg b^2/\lambda_{s2}$. The cosine term is due to the interference of two amplitudes passing through two slits, but modified by the imaginary phase from $s1$ photons which are not detected. The phase difference between two optical pathways is approximately equal to $\pi a x_2/\lambda_{s2}[d_1+(\omega_{s2}/\omega_u)z_2]$. The sinc terms in Eq. (46) represent the effects of nonzero width and length of the slits.

In Fig. 4, the ghost interference-diffraction patterns of a double slit are plotted as a function of transverse coordinates (x_2,y_2) of detector D2 with a different amount of transverse modes in the nondetected $s1$ beam. The double-slit aperture with slit width $b=0.1$ mm, distance between slits $a=0.5$ mm, and length of each slit $\ell=1$ mm is placed in the $s2$ beam at a distance $d_1=0.3$ m from the crystal. The $s2$ beam passes through it and then travels $d_1'=1$ m to detector D1 which is fixed on the axis of the $s2$ beam. The up-converted beam travels $z_2=1.8$ m freely from the crystal to detector D2. In the simulations, the wavelengths of two down-converted beams are taken as 870 nm and the wavelength of the up-conversion beam as 680 nm. In Fig. 4(a), since there are many transverse modes in the idle $s1$ beam, the ghost interference-diffraction pattern grows fat and loses the fidelity; while in Fig. 4(b), the pattern has a better resolution because there are few transverse modes in the $s1$ beam.

The physics can be understood as follows. Recall $\vec{\alpha}_0$ in Eq. (28). By setting $\vec{\rho}_1=0$, there remain two terms which determine the properties of this vector: the first term is associated with the spatial coordinates of detector D2 and the second one with the transverse modes in the $s1$ beam. The first integral in Eq. (46) determines the curvature along the x_2 axis and the second integral describes the behavior along the y_2 axis. When the transverse modes of the $s1$ beam are few, $\vec{\alpha}_0$ mainly characterizes the two~photon properties. It should be noted that the symbol "~" in this paper indicates the approximate two photons in triphoton and they are different from biphotons in SPDC or EIT-based systems. Increasing d_1 or/and z_2, the oscillation periods along the x_2 and y_2 axes are also increased as shown in Eq. (28).

Next, we consider this ghost interference-diffraction experiment by doing triphoton coincidence counting measurement and the double slit is only placed in the $s1$ beam (see Fig. 5). From Eq. (37), ignoring the constants it is easy to obtain

$$R_3^{tr}(x_2,y_2;x_3,y_3)=\cos^2\left(\frac{a\alpha_{03,x}}{2}\right)\mathrm{sinc}^2\left(\frac{b\alpha_{03,x}}{2}\right)\mathrm{sinc}^2\left(\frac{\ell\alpha_{03,y}}{2}\right). \tag{47}$$

Equation (47) has the same analogy as the double-slit interference-diffraction experiment done in SPDC. But the cosine term now turns out to be the interference of two *effective* amplitudes traveling through two slits. The detection should be also implemented at the far-field zone. In Fig. 6, the double-slit interference-diffraction pattern is sketched as the point detector D2 is fixed in the axis of the $s2$ beam while detector D3 is scanned in its transverse plane (x_3,y_3). The distance from the crystal to detector D2 is $z_2=1.6$ m and

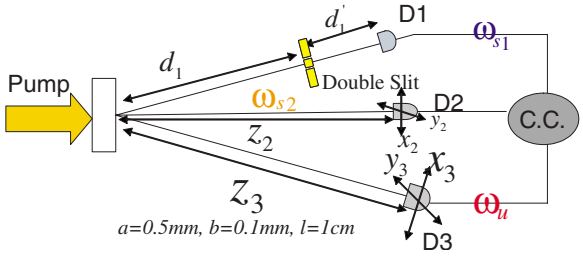

FIG. 5. (Color online) Triphoton ghost interference-diffraction experiment setup with one double slit. The double slit is inserted in the ω_{s1} beam and one scans the transverse planes of detectors D2 and D3.

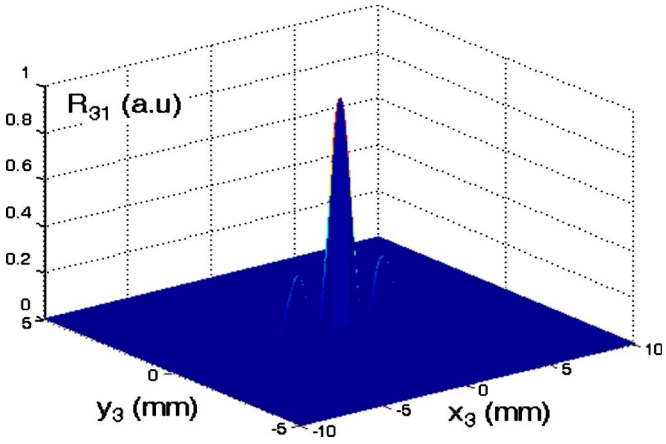

FIG. 6. (Color online) Ghost interference-diffraction pattern of a double slit in triphoton coincidence counting detection. x_3 and y_3 represent the spatial position of detector D3 and detector D2 is fixed in the axis of the $s2$ beam. The parameters were chosen as $d_1=0.3$ m, $z_2=1.6$ m, and $z_3=1.5$ m.

from the crystal to detector D3 is $z_3=1.5$ m. Comparing with Fig. 4, it is obvious that Fig. 6 gives a better interference-diffraction pattern, i.e., a better resolving power. To understand the behavior in this experimental setup, recall $\vec{\alpha}_{03}$ given in Eq. (34). By setting $\vec{\rho}_1=\vec{\alpha}_2=0$, $\vec{\alpha}_{03}$ is only a function of transverse coordinates of detector D3. The first two terms on the right-hand side in Eq. (34) describe the feature along the x_3 axis while the third term tells the curve along the y_3 axis. Increasing d_1 or/and $z_{2,3}$, the oscillation period along the x_3 axis is also increased and this can be understood by examining $\vec{\alpha}_{03}$ in Eq. (34). Until now the discussions are based on one double slit and we found that the ghost interference-diffraction patterns exhibit some similar features as those given by SPDC.

Now we turn to our major work: the two double-slit interference-diffraction experiment (see Fig. 7). For simplicity, we assume that two identical double-slit apertures are inserted into the system. One double slit is inserted in the $s1$ down-converted beam and the other in the up-converted beam. Equation (40) now takes the form

$$
\begin{aligned}
A_{32}^{tr}(\vec{\alpha}_1,\vec{\alpha}_2) = b\ell\left(\int_{-a-b/2}^{-a+b/2} dx_1 + \int_{a-b/2}^{a+b/2} dx_1\right) \\
\times e^{-ix_1\alpha_{1x}}\left[e^{ia\alpha_{2x}/2}e^{ix_1(a/2l^2-\alpha_{1x})}\right. \\
\left. + e^{-ia\alpha_{2x}/2}e^{-ix_1(a/2l^2+\alpha_{1x})}\right] \\
\times \mathrm{sinc}\left[\frac{b}{2}\left(\alpha_{2x}+\frac{x_1}{l^2}\right)\right]\int_{-\ell/2}^{\ell/2} dy_1 e^{-iy_1\alpha_{1y}} \\
\times \mathrm{sinc}\left[\frac{\ell}{2}\left(\alpha_{2y}+\frac{y_1}{l^2}\right)\right], \qquad (48)
\end{aligned}
$$

where we have decomposed all the vectors in their transverse planes, (x,y). To understand the role of the crossed phase term in Eq. (40), we will discuss the Young's experiments with two double slits in three regions. To simplify the discussions, we take $\vec{\rho}_1=\vec{\rho}_2=0$, i.e., two detectors D1 and D2 are fixed at their corresponding axes, so that the triphoton coincidence counting rate is simply the function of spatial coordinates of detector D3, $\vec{\rho}_3=(x_3,y_3)$. First, we set $z_3 \ll d_{1,2}$ and in this case, the crossed phase term in Eq. (40) plays an unimportant role for determining the ghost interference-diffraction pattern. In Fig. 8(a), the pattern is depicted by choosing $d_1=d_2=2.1$ m and $z_3=0.3$ m. The picture looks like that shown in Fig. 6 (or Fig. 4) except the fringes are suppressed. The picture can be understood by following the analysis presented above. Second, if now z_3 is comparable with $d_{1,2}$, the crossed phase term is as important as another two phase term in Eq. (40) and they together determine the interference-diffraction pattern. In Fig. 8(b), by choosing $d_1=d_2=1.4$ m and $z_3=1.6$ m, we found that the interference-diffraction pattern is getting broadened and the modulation has a slower period. Third, by setting $z_3 \gg d_{1,2}$, the crossed phase term now has an important contribution to A_{32}^{tr}. In Fig. 8(c), we show one example in which $d_1=d_2=0.25$ m and $z_3=2$ m. In Fig. 8(d), we choose $d_1=d_2=0.2$ m and $z_3=1.8$ m. As we see, the oscillations along the x_3 axis are different from those demonstrated in Figs. 8(a) and 8(b): around $x_3=0$, the maximum shown in Figs. 8(a) and 8(b) now tends to disappear and it appears unsymmetrically besides the center. The new distribution is due to the interference of two amplitudes crossing through two double slits. The unsymmetrical distribution is because the ratio of $[(\omega_{s1}/d_1)/(\omega_u/d_2)]$ is not equal to one. When this ratio goes to one, the center of the feature moves toward $x_3=0$. In addition, by making $z_3/d_{1,2} \gg 1$, the center of the coincidences R_{32}^{tr} approaches zero. This is the essential difference between biphoton optics and triphoton optics. The oscillation periods along the x_3 and y_3 axes alter following the changes of $d_{1,2}$ and z_3. To know the detailed changes, one may apply the above procedure by examining the properties of $\vec{\alpha}_{1,2}$ and l given in Eq. (41). Of course, there is no classical correspondence, no matter quantum imaging or quantum interference-diffraction phenomena as we discussed in this paper.

Knowing the interference-diffraction patterns of two double slits, one may raise a simple question: by placing two single slits in Fig. 7 (instead of double slits) in two arms, what can we observe? To answer this question, let us consider an experiment where two identical slits together form the aperture function given in Eq. (45). Following the same procedure, one may find that the two-image-amplitude in Eq. (44) becomes

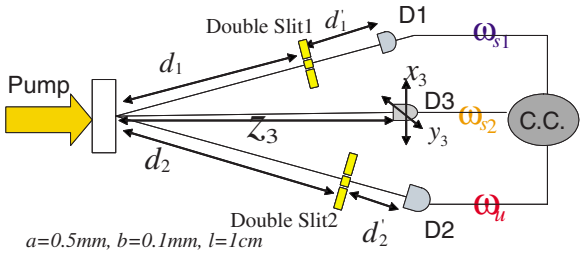

FIG. 7. (Color online) Triphoton ghost interference-diffraction experiment setup with two double slits. Two double slits are inserted in the ω_{s1} and ω_u beams, respectively. Detector D3 is scanned in its transverse plane (x_3,y_3) to do the triphoton coincidence measurement.

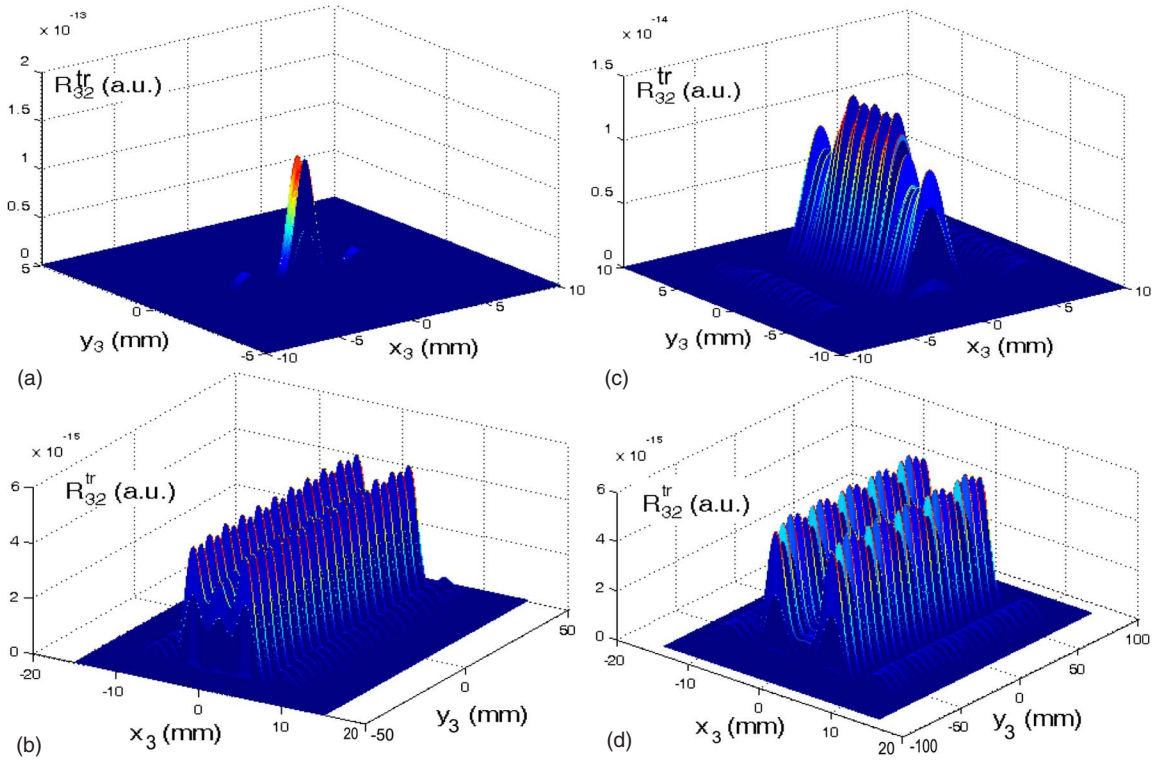

FIG. 8. (Color online) Ghost interference-diffraction patterns of two double slits in triphoton coincidence counting measurement. x_3 and y_3 represent the position of detector D3. The parameters were chosen as (a) $d_1=d_2=2.1$ m and $z_3=0.3$ m; (b) $d_1=d_2=1.4$ m and $z_3=1.6$; (c) $d_1=d_2=0.25$ m and $z_3=2$ m; and (d) $d_1=d_2=0.2$ m and $z_3=1.8$ m.

$$\mathcal{S}(x_3,y_3)=\int_{a-b}^{a+b}dx_2\ \mathrm{sinc}\left[b\left(\alpha_{1x}+\frac{x_2}{l^2}\right)\right]\times e^{ix_2(a/l^2-\alpha_{2x})}\int_{\ell/2}^{\ell/2}dy_2\ \mathrm{sinc}\left[\frac{\ell}{2}\left(\alpha_{1y}+\frac{y_2}{l^2}\right)\right]e^{-iy_2\alpha_{2y}}. \tag{49}$$

As we see, Eq. (49) exactly has the similar sequence as Eq. (48); the two slits play the role as one double slit. Though there are also some oscillations in the y_3 direction, they are difficult to observe in the experiment.

V. DISCUSSION AND SUMMARY

In summary, we have presented a detailed analysis of the transverse correlation of a triphoton state generated from two SPDCs and one SFG within a single crystal as proposed in Ref. [18]. For simplicity, we have assumed that the pump beam is a monochromatic plane wave traveling along the longitudinal axis without any depletion. We have discussed the triphoton geometrical and physical optics, with emphasis on the roles of the spectral function F and classical transfer functions g. For the emergence of quantum imaging, we have studied three classes: single-photon detection, two~photon, and three-photon coincidence counting rates. Our results show that the singles counts have no structure in experiments such as the ghost interference experiment [11]. In the two ~photon coincidence counting measurement, the GTLE is recovered as implemented by SPDC sources. However, the quality of the image becomes worse if more transverse modes are generated in the triphoton state. This is because the point-point relationship between the object and image is modified by the transverse modes in the untouched beam. For the triphoton coincidence counting measurement, if only one object with one lens is placed in the optical beam, the ghost image governed by the modified GTLE has a better resolution as in the SPDC case, and the point-point correspondence between the object and image is well-defined. The distance between the imaging plane and lens is a parallel combination of distances between two detectors and a lens weighted by the ratio of free-space wavelengths, which behaves as the parallel combination of resistors in the electromagnetism theory. The positions of two remaining detectors are not unique. The situation changes dramatically if two OSs are inserted into two optical beams. In such a case, the general conclusion about the imaging could not be drawn because the point-point correspondence for forming images is not well-defined, even though the GTLEs are satisfied. To characterize such a situation, a two-image-amplitude Fourier transform [Eq. (44)] is defined. Whether the point-point relation between object and image is restored to some extent, depends on the impact of the crossed phase term in Eq. (44). In general, one image washes out the other one so that in triphoton coincidences, no image can be observed. However, under some conditions two roughly dependent images can be formed in the imaging planes. To further understand the transverse correlation in triphoton entanglement, we have also studied the triphoton physical optics by looking at the

double-slit interference-diffraction experiments under different setups. With only one double slit, the interference-diffraction pattern can be understood from the biphoton picture. However, when placing two double slits in the system, the pattern shows different features. There is a destructive interference occurrence between two amplitudes crossing two double slits. This is the essential difference between biphoton optics and triphoton optics. We also demonstrated that the modified Klyshko's advanced-wave model provides an intuitive picture to understand the triphoton geometrical and physical optics.

In the discussions, for simplicity, we have decoupled the interlocking between spatial and temporal coherence. This simplification allows us to focus on the main features caused by the spatial correlations and we do not worry about the longitudinal manifestation. The generalization of quantum ghost imaging in multiphoton entanglement is beyond the scope of this paper and will be presented elsewhere [21]. It should be also pointed out that the calculations in this paper are carried out at the single-photon level. When this limitation is broken, one may choose solving the three-dimensional Maxwell's equations to study the spatial correlations, as discussed in [22,23].

ACKNOWLEDGMENTS

The authors are grateful to Shining Zhu and Guiliano Scarcelli for helpful discussions about the context presented in this paper. J.-M. Wen, M. H. Rubin, and Y.-H. Shih were supported in part by the U.S. Army Research Office MURI Grant No. W911NF-05-1-0197. P. Xu (and S. N. Zhu) acknowledges the financial support of the State Key Program for Basic Research of China (2004CB619003) and the National Natural Science Foundation of China (Grant No. 10534020).

APPENDIX A: GREEN'S FUNCTIONS

The propagation of free-space electric fields is described by the Green's function. In this appendix, we give a brief review of properties of Green's functions for an electric field through a diffraction limited linear optical system, which can be in terms of an aperture function, following the treatment in [10]. As pictured in Fig. 2 the aperture function, defined by $s(\vec{\rho}_s)$, is placed in a plane a distance d_1 from the output surface of the crystal and d_1' from the detector. The Green's function is given by

$$g_1(\vec{\alpha},\omega,\vec{\rho}_1,z_1)=\int d^2\rho_s \int d^2\rho_c \varphi(\vec{\rho}_1-\vec{\rho}_s,d_1') \times s_1(\vec{\rho}_s)\varphi(\vec{\rho}_s-\vec{\rho}_c,d_1)e^{i\vec{\alpha}\cdot\vec{\rho}_c}, \tag{A1}$$

where $z_1=d_1+d_1'$ and the optical transfer function is defined in the paraxial approximation by [24]

$$\varphi(\vec{\rho},d)=\frac{-i\omega}{2\pi c}\frac{e^{i\omega d/c}}{d}\psi\left(\vec{\rho},\frac{\omega}{cd}\right), \tag{A2}$$

$$\psi\left(\vec{\rho},\frac{\omega}{cd}\right)=e^{i\omega\rho^2/2cd}. \tag{A3}$$

It is useful to note that [25]

$$\psi^*\left(\vec{\rho},\frac{\omega}{cd}\right)=\psi\left(\vec{\rho},-\frac{\omega}{cd}\right), \tag{A4}$$

$$\psi\left[\vec{\rho},\frac{\omega}{c}\left(\frac{1}{d}+\frac{1}{d'}\right)\right]=\psi\left(\vec{\rho},\frac{\omega}{cd}\right)\psi\left(\vec{\rho},\frac{\omega}{cd'}\right), \tag{A5}$$

$$\psi\left(|\vec{\rho}-\vec{\rho}'|,\frac{\omega}{cd}\right)=\psi\left(\vec{\rho},\frac{\omega}{cd}\right)\psi\left(\vec{\rho}',\frac{\omega}{cd}\right)e^{-i\omega/cd\vec{\rho}\cdot\vec{\rho}'}, \tag{A6}$$

and the Fourier transform equation is

$$\int d^2\rho\psi\left(\vec{\rho},\frac{\omega}{cd}\right)e^{i\vec{\alpha}\cdot\vec{\rho}}=i\frac{2\pi cd}{\omega}\psi\left(\vec{\alpha},-\frac{cd}{\omega}\right). \tag{A7}$$

It is easy to show that

$$g_1(\vec{\alpha},\omega,\vec{\rho}_1,z_1)=\frac{-i\omega d_1'}{2\pi c}e^{i\omega z_1/c}\psi\left(\vec{\rho}_1,\frac{\omega}{cd_1'}\right) \times S_1\left(\vec{\alpha}-\frac{\omega}{cd_1'}\vec{\rho}_1,\frac{\omega}{cd_1'}\right)\psi\left(\vec{\alpha},-\frac{cd_1}{\omega}\right), \tag{A8}$$

$$S_1\left(\vec{\alpha}-\frac{\omega}{cd_1'}\vec{\rho}_1,\frac{\omega}{cd_1'}\right)=\int d^2\rho_s\psi\left(\vec{\rho}_s,\frac{\omega}{cd_1'}\right)e^{i(\vec{\alpha}-\omega/cd_1'\vec{\rho}_1)\cdot\vec{\rho}_s}s_1(\vec{\rho}_s). \tag{A9}$$

If we place a converging lens of focal length f in the plane of the aperture function, then

$$s_1(\vec{\rho}_s)=\psi\left(\vec{\rho}_s,-\frac{\omega}{cf}\right)t(\vec{\rho}_s), \tag{A10}$$

where $t(\vec{\rho}_s)$ is the transmission function of the aperture. By using Eq. (A9) we have

$$S_1\left(\vec{\alpha}-\frac{\omega}{cd_1'}\vec{\rho}_1,\frac{\omega}{cd_1'}\right)=\int d^2\rho_s e^{i(\vec{\alpha}-\omega/cd_1'\vec{\rho}_1)\cdot\vec{\rho}_s}t(\vec{\rho}_s), \tag{A11}$$

which is the Fourier transform of $t(\vec{\rho}_s)$.

Similarly, we can find that the Green's function

$$g_2(\vec{\alpha},\omega,\vec{\rho}_2,z_2)=e^{i\omega z_2/c}\psi\left(\vec{\alpha},-\frac{cz_2}{\omega}\right)e^{i\vec{\alpha}\cdot\vec{\rho}_2}. \tag{A12}$$

These results have been frequently applied in the context.

APPENDIX B: FOURIER TRANSFORM OF PRODUCT OF TWO SINC FUNCTIONS

In Eq. (25) we have defined the function $\wedge(\tau,a,b,c,d;\nu)$, which is the Fourier transform of product of two sinc functions,

$$\int d\nu e^{-i\nu\tau}\,\mathrm{sinc}\left[\frac{(\nu-a)c}{2}\right]\mathrm{sinc}\left[\frac{(\nu-b)d}{2}\right]$$

$$=\frac{\sqrt{2}\pi}{(b-a)cd}e^{-i\pi/4}\{e^{i[b\tau+c(b-a)/2]}[\mathrm{signum}(\tau+c/2-d/2)-\mathrm{signum}(\tau+c/2+d/2)]+e^{i[a\tau+d(b-a)/2]}$$
$$\times[\mathrm{signum}(\tau-c/2-d/2)-\mathrm{signum}(\tau+c/2-d/2)]+e^{i[b\tau-c(b-a)/2]}[\mathrm{signum}(\tau-c/2+d/2)-\mathrm{signum}(\tau-c/2-d/2)]$$
$$+e^{i[a\tau-c(b-a)/2]}[\mathrm{signum}(\tau+c/2+d/2)-\mathrm{signum}(\tau-c/2+d/2)]\},\tag{B1}$$

where $\mathrm{signum}(x)=x/|x|$.

[1] A. Einstein, B. Podolsky, and N. Rosen, Phys. Rev. **47**, 777 (1935).

[2] E. Schrödinger, Naturwiss. **23**, 807 (1935); **23**, 823 (1935); **23**, 844 (1935) [translation in *Quantum Theory of Measurement*, edited by J. A. Wheeler and W. H. Zurek (Princeton University Press, Princeton, 1983)].

[3] D. N. Klyshko, *Photons and Nonlinear Optics* (Gordon and Breach, New York, 1988); Y.-H. Shih, Rep. Prog. Phys. **66**, 1009 (2003); L. Mandel, Rev. Mod. Phys. **71**, S274 (1999); A. Zeilinger, *ibid.* **71**, S288 (1999); M. H. Rubin, D. N. Klyshko, Y.-H. Shih, and A. V. Sergienko, Phys. Rev. A **50**, 5122 (1994).

[4] V. Balić, D. A. Braje, P. Kolchin, G. Y. Yin, and S. E. Harris, Phys. Rev. Lett. **94**, 183601 (2005); P. Kolchin, S. Du, C. Belthangady, G. Y. Yin, and S. E. Harris, *ibid.* **97**, 113602 (2006); J.-M. Wen and M. H. Rubin, Phys. Rev. A **74**, 023808 (2006); **74**, 023809 (2006); S. Du, J.-M. Wen, M. H. Rubin, and G. Y. Yin, Phys. Rev. Lett. **98**, 053601 (2007); J.-M. Wen, S. Du, and M. H. Rubin, Phys. Rev. A **75**, 033809 (2007); 76, 013825 (2007).

[5] Y.-H. Shih and C. O. Alley, Phys. Rev. Lett. **61**, 2921 (1988); P. G. Kwiat, K. Mattle, H. Weinfurter, A. Zeilinger, A. V. Sergienko, and Y.-H. Shih, *ibid.* **75**, 4337 (1995).

[6] A. Migdall, R. Datla, A. V. Sergienko, J. S. Orszak, and Y.-H. Shih, Appl. Opt. **37**, 3455 (1998).

[7] B. E. A. Saleh, B. M. Jost, H.-B. Fei, and M. C. Teich, Phys. Rev. Lett. **80**, 3483 (1998).

[8] A. V. Belinskii and D. N. Klyshko, J. Exp. Theor. Phys. **78**, 259 (1994); P. H. S. Ribeiro, S. Padua, J. C. MachadodaSilva, and G. A. Barbosa, Phys. Rev. A **49**, 4176 (1994).

[9] T. B. Pittman, Y.-H. Shih, D. V. Strekalov, and A. V. Sergienko, Phys. Rev. A **52**, R3429 (1995).

[10] M. H. Rubin, Phys. Rev. A **54**, 5349 (1996).

[11] D. V. Strekalov, A. V. Sergienko, D. N. Klyshko, and Y.-H. Shih, Phys. Rev. Lett. **74**, 3600 (1995).

[12] A. N. Boto, P. Kok, D. S. Abrams, S. L. Braunstein, C. P. Williams, and J. P. Dowling, Phys. Rev. Lett. **85**, 2733 (2000).

[13] M. D'Angelo, M. V. Chekhova, and Y.-H. Shih, Phys. Rev. Lett. **87**, 013602 (2001).

[14] A. K. Ekert, Phys. Rev. Lett. **67**, 661 (1991); N. Gisin, G. Ribordy, W. Tittel, and H. Zbinden, Rev. Mod. Phys. **74**, 145 (2002).

[15] D. M. Greenberger, M. A. Horne, and A. Zeilinger, in *Bell's Theorem, Quantum Theory, and Conceptions of the Universe*, edited by M. Kafatos (Kluwer Academics, Dordrecht, The Netherlands, 1989), p. 73; Phys. Today **46** (8), 22 (1993).

[16] C. H. Bennett, Phys. Today **48**(10), 24 (1995); S. L. Braunstein and A. Mann, Phys. Rev. A **51**, R1727 (1995).

[17] Y.-H. Shih and M. H. Rubin, Phys. Lett. A **182**, 16 (1993); M. Zukowski, A. Zeilinger, M. A. Horne, and A. K. Ekert, Phys. Rev. Lett. **71**, 4287 (1993); D. N. Klyshko, Phys. Lett. A **172**, 399 (1993); P. van Loock and S. L. Braunstein, Phys. Rev. Lett. **84**, 3482 (2000); O. Pfister, S. Feng, G. Jennings, R. Pooser, and D. Xie, Phys. Rev. A **70**, 020302(R) (2004).

[18] T. E. Keller, M. H. Rubin, Y.-H. Shih, and L.-A. Wu, Phys. Rev. A **57**, 2076 (1998).

[19] D. N. Klyshko, Phys. Lett. A **128**, 133 (1988); Sov. Phys. Usp. **31**, 74 (1988) [Usp. Fiz. Nauk **154**, 133 (1988)].

[20] P. Xu, S. H. Ji, S. N. Zhu, X. Q. Yu, J. Sun, H. T. Wang, J. L. He, Y. Y. Zhu, and N. B. Ming, Phys. Rev. Lett. **93**, 133904 (2004).

[21] J.-M. Wen, Ph.D. dissertation, UMBC, 2007 (unpublished).

[22] J.-M. Wen and M. H. Rubin, Phys. Rev. A **74**, 023809 (2006).

[23] E. Brambilla, A. Gatti, M. Bache, and L. A. Lugiato, Phys. Rev. A **69**, 023802 (2004); O. Jedrkiewicz, Y.-K. Jiang, E. Brambilla, A. Gatti, M. Bache, L. A. Lugiato, and P. Di Trapani, Phys. Rev. Lett. **93**, 243601 (2004).

[24] J. W. Goodman, *Introduction to Fourier Optics* (McGraw-Hill, New York, 1968).

[25] A. VanderLugt, *Optical Signal Processing* (Wiley, New York, 1992).